International Conference on Mathematics and Computational Methods Applied to Nuclear Science and Engineering (M&C 2011)
Rio de Janeiro, RJ, Brazil, May 8-12, 2011, on CD-ROM, Latin American Section (LAS) / American Nuclear Society (ANS)
ISBN 978-85-63688-00-2

ANOMALOUS BEHAVIOUR OF THERMOPHYSICAL PROPERTIES OF STOICHIOMETRIC URANIUM DIOXIDE BY MOLECULAR DYNAMICS SIMULATION

Lunev A.V., Tarasov B.A., Nazarov A.V.
National Research Nuclear University MEPhI
Kashirskoye Shosse, 31, Moscow - 115409, Russian Federation
alounev@list.ru; ulens.up@gmail.com; avn46@mail.ru

ABSTRACT

We present a classical molecular dynamics simulation of uranium dioxide in the temperature range of 300-3000 K. Temperature dependences of thermal conductivity, heat capacity and ionic conductivity are investigated. Our study shows the rise of thermal conductivity of uranium dioxide at very high temperatures (above 2500 K), which is not predicted by the former anharmonic theories. Several pair potentials are used in the simulation, and they depict similar effects. Long-range forces are accounted by Ewald sums. Static thermal properties are evaluated in NPT ensemble. It is shown that a high-temperature peak on heat capacity is present and is more legible in large systems. To ensure the best reliability, transport properties are evaluated using the theory of autocorrelation functions in NVE ensemble. In order to properly define thermal conductivity in ionic systems with charge fluxes, an expression which accounts the thermoelectric effect is derived from Onsager reciprocal relations. The rise on temperature dependence of thermal conductivity is accompanied by the peak on heat capacity and an anomalous rise of ionic conductivity. However, it is shown that there is no partial melting of the oxygen sublattice, which suggests that the system doesn't necessarily exhibit a superionic transition. Instead, kick-out diffusion in oxygen sublattice is proposed to be the origin of such anomalous behavior of thermophysical properties.

Key Words: uranium dioxide, thermal conductivity, heat capacity, ionic conductivity.

1. INTRODUCTION

There is a tendency to increase the operating temperature of nuclear reactors. This means that the themophysical properties of nuclear fuels at high temperatures grow in importance. Most reactors, either already operating or to-be-constructed, use uranium dioxide (UO_2) as fuel. Although there is a large number of experimental data available, most of it relates to temperatures below 2000 K. Above this temperature there are considerable discrepancies in data due to the complexity of experiments. Most debates are centered on the high-temperature behavior of thermal conductivity: whether there is a rise in thermal conductivity or not.

Existing theories are unable to explain this behavior unambiguously. Most suppose there is a polaron or ambipolar contribution in thermal conductivity, yet there are no clear evidences of this to be true. The radiative component also remains only as a hypothesis.

There is a phenomenon, however, which may be related to the rise of thermal conductivity as well. It relates to the so-called superionic transition. The main idea behind this is that Frenkel disorder may happen in uranium dioxide at high temperatures inducing a peak on the heat capacity at ~ 2670 K [1]. We think the question on the reasons behind such behavior is still open. In this paper we investigate this phenomenon more thoroughly.

Nevertheless, if oxygen is so mobile at high temperatures, lattice thermal conductivity can't be reduced to the Debye law. This is mainly because if ionic displacements are large, one is unable to write Taylor expansion of the potential energy, so there is no point in speaking of anharmonicity.

It is clear that the kinetic equation theory can't deal with such complexities. There doesn't seem to be a way of investigating this problem by common analytical methods. The solution lies in using molecular dynamics simulation along with nonequilibrium statistical mechanics equations.

The theory of autocorrelation functions offers a strict expression for deriving thermal conductivity of a system near equilibrium – the Green-Kubo relations [2]. Our work is centered on calculation of kinetic properties of UO_2 using this method. In addition we present the results on static thermal properties.

2. SIMULATION MODEL

The perfect crystal of stoichiometric uranium dioxide has a fluorite unit cell, depicted on fig. 1. FCC positions of the outer cube are occupied by U^{4+} ions, and O^{2-} ions are the vertices of the inner cube.

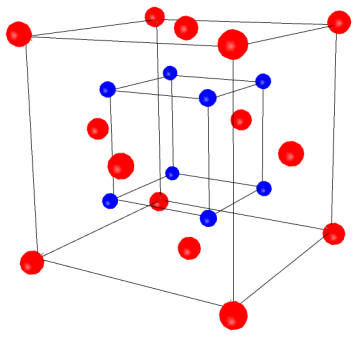

Figure 1. UO2 unit cell. Red spheres are U^{4+} ions, and blue spheres are O^{2-} ions.

The calculation cell includes a number of unit cells and an additional layer in each of three spatial directions that maintains the 2:1 ratio between oxygen and uranium ions. Periodic

boundary conditions are used with minimal image convention conditions. Initial random velocities are chosen for each ion so that the initial system temperature is $2T_0$.

2.1. Potentials

We use the potential functions given by Arima [3],[5], Basak [4] and Yakub [6]. Two potential forms are considered:

$$U_{ij}(r) = K_e \frac{z_i z_j}{r} + f_0(b_i + b_j) \exp\left(\frac{a_i + a_j - r}{b_i + b_j} \right) - \frac{c_i c_j}{r^6} + D_{ij} \left(\left[\exp(-\beta_{ij} \left(r - r_{ij}^* \right) - 1 \right]^2 - 1 \right) \tag{1}$$

$$U_{ij}(r) = K_e \frac{q_i q_j}{r} + A_{ij} \exp\left(-\frac{r}{\rho_{ij}} \right) - \frac{C_{ij}}{r^6} \tag{2}$$

The potential parameters appearing in eq. (1) and (2) are given in the original papers of the authors. We note that we use four potential parameters sets. Arima1 is a type (2) potential, Arima2, Basak and Yakub are type (1) potentials. Only Yakub and Basak potentials account for covalence contribution to U-O ionic bond.

Each potential type has a long-range and a short-range part. Coulombic term, if accounted for directly, gives rise to divergence in lattice sums. A common method to deal with such a problem is to break the summation on a real space and a reciprocal space parts. To speed up the calculation we use the following expressions for the Coulombic sums [7]:

$$\begin{aligned} U_C &= \frac{1}{2} \sum_{\mathbf{K} \neq 0} E_{\mathbf{K}} + K_e \sum_i \sum_{j<i} z_i z_j \frac{erfc\left(\omega r_{ij} \right)}{r_{ij}} - K_e \frac{\omega}{\sqrt{\pi}} \sum_i z_i^2; \\ E_{\mathbf{K}} &= \frac{4\pi}{V} K_e \left[\frac{1}{k^2} \exp\left(-\frac{k^2}{4\omega^2} \right) \right] \times \left[\left\{ \sum_i z_i \cos(\mathbf{k} \cdot \mathbf{r}_i) \right\}^2 + \left\{ \sum_i z_i \sin(\mathbf{k} \cdot \mathbf{r}_i) \right\}^2 \right] \end{aligned} \tag{3}$$

$$\begin{aligned} \mathbf{F}_i &= -\sum_j \frac{\partial U}{\partial \mathbf{r}_{ij}} = \frac{2\pi}{V} K_e z_i \sum_{\mathbf{K} \neq 0} \left[\frac{\mathbf{K}}{K^2} \exp\left(-\frac{K^2}{4\omega^2} \right) \right] \times \\ &\times \left[\sin(\mathbf{K} \cdot \mathbf{r}_i) \sum_j z_j \cos(\mathbf{K} \cdot \mathbf{r}_j) - \cos(\mathbf{K} \cdot \mathbf{r}_i) \sum_j z_j \sin(\mathbf{K} \cdot \mathbf{r}_j) \right] + \\ &+ \sum_i \sum_{j>i} z_i z_j K_e \frac{1}{r_{ij}} \left[\frac{erfc\left(\omega r_{ij} \right)}{r_{ij}} - \frac{2\omega}{\sqrt{\pi}} \exp\left(-\omega^2 r_{ij}^2 \right) \right] \cdot \frac{\mathbf{r}_{ij}}{r_{ij}} \end{aligned} \tag{4}$$

Eq. (3) is an expression for calculating the total electrostatic energy of the system. Here ω is Ewald's splitting parameter; $r_{ij} \equiv \left|\mathbf{r}_{ij}\right| = \left|\mathbf{r}_i - \mathbf{r}_j\right|$; K_e is the electrostatic constant in Colomb law; V is the volume of calculation cell. Eq. (4) is a derivative of eq. (3) and represents the force acting on the ion *i*. The sums in the reciprocal space are over all ions of the calculation cell, and the sum in real space accounts also for the images.

Both in real and reciprocal spaces cut-offs are used. Expression matching the corresponding parameters can be found elsewhere [7]. Summation which relates to the short-range parts in eq. (1) and (2) are simply accounted for in a cut-off sphere with a radius of a half of the cell's length. Pressure *P* is calculated using the virial theorem in the following form [7]:

$$3PV = \sum_k \frac{p_k^2}{m_k} + \sum_i \sum_{j>i} \mathbf{F}_{ij}^{real} \cdot \mathbf{r} + \sum_{\mathbf{K}} \frac{E_{\mathbf{K}}}{2} \left(1 - \frac{K^2}{2\omega^2}\right) \tag{5}$$

Here p_k and m_k are momentum and mass of *k*-th ion. $\mathbf{F}_{ij}^{real}$ is the real-space part of the force (both long- and short-range).

2.2. Ensembles

Calculations are made in two ensembles: NPT and NVE. The first is used to obtain static thermal properties which are less liable to the form of fluctuations spectrum. Transport properties are evaluated in NVE ensemble. We use the following set of equations for NPT ensemble [8]:

$$\begin{cases} \mathbf{r}_{i\alpha} = \dfrac{\mathbf{p}_{i\alpha}}{m_{i\alpha}} + \eta\left(\mathbf{r} - \mathbf{R}_0\right), \quad \mathbf{p}_{i\alpha} = \mathbf{F}_{i\alpha} - \left(\eta + \xi_\alpha\right)\mathbf{p}_{i\alpha}, \\ \xi_\alpha = \nu_{T_\alpha}^2 \left(\dfrac{T_\alpha(t)}{T_0} - 1\right), \quad \dot{\eta} = \dfrac{\nu_P^2}{N_\alpha k_B T_0} V\left(P(t) - P_0\right), \quad \dot{V} = 3V\eta \end{cases} \tag{6}$$

For each sublattice with its own α unique values of $\nu_{T_\alpha}^2$ and ν_P^2 exist. The first is the frequency of thermostat coupling, and the second – of the barostat. The coupling between baro- and thermostat and the system is done by including frictional forces $\eta\mathbf{p}_{i\alpha}$ and $\xi_\alpha\mathbf{p}_{i\alpha}$ correspondingly. N_α is the number of ions in α sublattice.

Equations of motion in NVE ensemble are simple Newtonian equations without constraints:

$$\frac{d\mathbf{p}_i}{dt} = \mathbf{F}_i, \quad \frac{d\mathbf{r}_i}{dt} = \frac{\mathbf{p}_i}{m_i} \tag{7}$$

Integration of eq. (6) and (7) are performed using velocity Verlet algorithm (and the corrected velocity Verlet algorithm for eq. (6) – see [8]).

2.3. Transport Properties in Non-equilibrium Statistical Mechanics

In ionic systems with mobile ions temperature gradients give rise to electric potential fluxes, so that thermoelectric effects must be accounted for. It can be shown that in this case thermal conductivity must be calculated using the following expression [9]:

$$\lambda = \frac{1}{T^2}\left(L_{QQ} - \frac{L_{QE}^2}{L_{EE}} \right) \tag{8}$$

Here $L_{\alpha\beta}$ are Onsager terms in the theory of irreversible processes. They can be defined using the following relations obtained in the theory of autocorrelation functions [9]:

$$L_{QQ} = \frac{V}{3k_B}\int_0^\infty \left\langle \mathbf{J}_Q(t)\cdot\mathbf{J}_Q(0)\right\rangle dt \tag{9}$$

$$L_{QE} = \frac{V}{3k_B}\int_0^\infty \left\langle \mathbf{J}_Q(t)\cdot\mathbf{J}_Z(0)\right\rangle dt \tag{10}$$

$$L_{EE} \equiv \sigma T = \frac{V}{3k_B}\int_0^\infty \left\langle \mathbf{J}_z(t)\cdot\mathbf{J}_z(0)\right\rangle dt \tag{11}$$

L_{EE} is related to the electric conductivity σ. Heat flux $\mathbf{J}_Q$ and electric flux $\mathbf{J}_z$ are given by [2]:

$$\mathbf{J}_Q = \frac{1}{V}\left\{ \sum_i E_i \frac{\mathbf{p}_i}{m_i} + \frac{1}{2m_i}\sum_{i<j}\left[\left(\mathbf{p}_i + \mathbf{p}_j\right)\cdot\mathbf{F}_{ij} \right]\mathbf{r}_{ij} \right\} \tag{12}$$

$$\mathbf{J}_z = \frac{1}{V}\sum_i \frac{z_i}{m_i}\mathbf{p}_i \tag{13}$$

Eq. (9) – (11) contain autocorrelation functions $\left\langle \mathbf{J}_\alpha(t)\cdot\mathbf{J}_\beta(0)\right\rangle$ in the ensemble average sense. In calculations it is convenient to use time averages. This is done by using the ergodic hypothesis. The procedure of such calculations is described elsewhere [10].

3. RESULTS

3.1. NPT Ensemble

We begin with the simulation by calculating static thermal properties.

The results of lattice parameter calculation with all four potentials are presented on fig. 2.

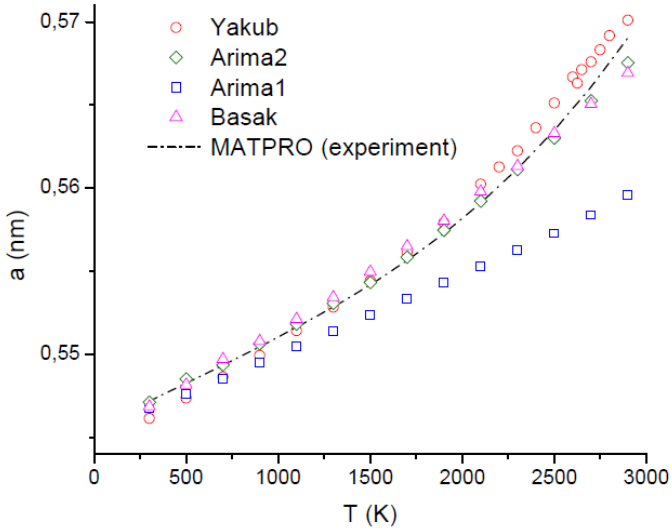

Figure 2. Temperature dependence of lattice parameter of UO_2. Experimental data taken from [11].

Lattice parameter was calculated as the averaged value of $n^{-1}V^{1/3}$ (n is the number of unit cells in each spatial direction) after reaching equilibrium. Initial equilibration took about 20×10^3 time steps. The time step corresponds to $80^{-1}\tau_D$ which is equivalent to 1 fs (τ_D is the inverse Debye frequency). System size was 5x5x5 (1500 ions). Tests were carried to show that increasing the number of ions doesn't change the obtained results.

Also, the heat capacity at constant pressure was calculated as $C_p = \frac{dH}{dT}$. The results are shown on fig. 3. Because we were most interested in Yakub and Arima2 potentials, we do not present the results on other potentials. In order to understand whether the high-temperature peak for Yakub potential on fig. 3 has physical meaning, we calculated heat capacity for a large system of 6144 ions (8x8x8). It is clearly shown that the peak is more distinct. A simple theoretical estimate of the heat capacity caused by phonons given by $C_p(T) = 3gR\cdot\left[1+3\alpha\gamma T\right]$ (where g is the number of molecular units per unit cell, α is the thermal expansion coefficient and γ is the Grueneisen parameter) is also plotted on the graph.

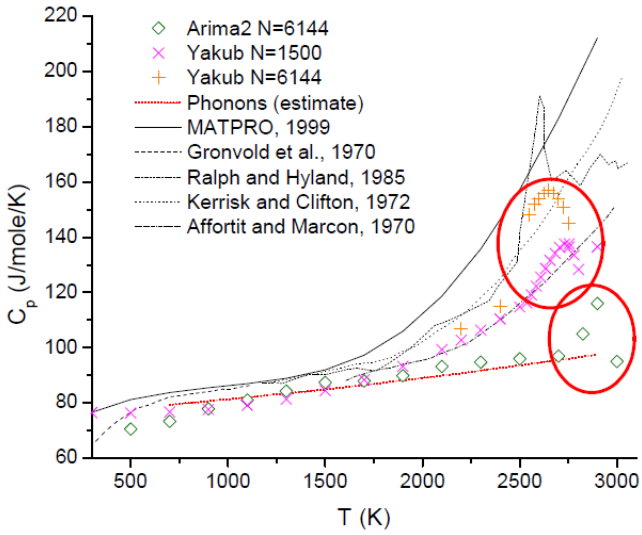

Figure 3. Temperature dependence of heat capacity at constant pressure of UO_2. Experimental data taken from [12].

3.2. NVE Ensemble

Calculations of transport properties are made in NVE ensemble. Long runs with more than 1×10^5 steps were made in a 6x6x6 system (2592 ions). Initial volume was calculated from the data of fig. 2. Initial equilibration took about a thousand step. After equilibration the autocorrelation function was calculated averaging on more than 1×10^4 time origins. Results for thermal conductivity calculation using eq. (8) are presented on fig. 4 for medium temperatures and on fig. 5 for high temperatures.

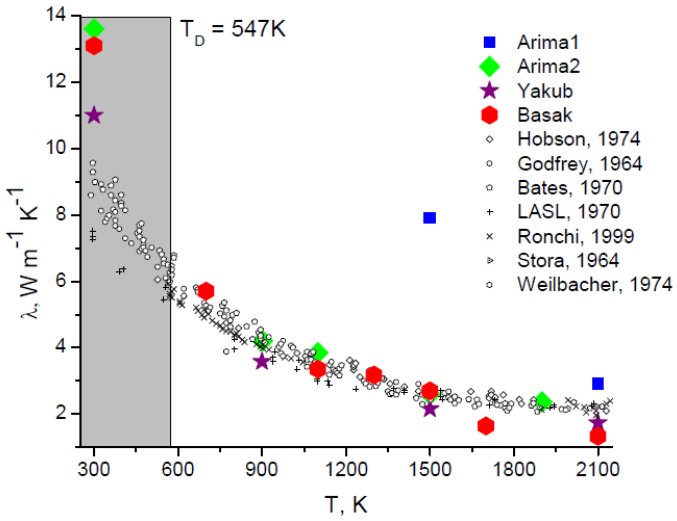

Figure 4. Thermal conductivity of stoichiometric UO_2 in the range of 300-2100K. Experimental data taken from [13].

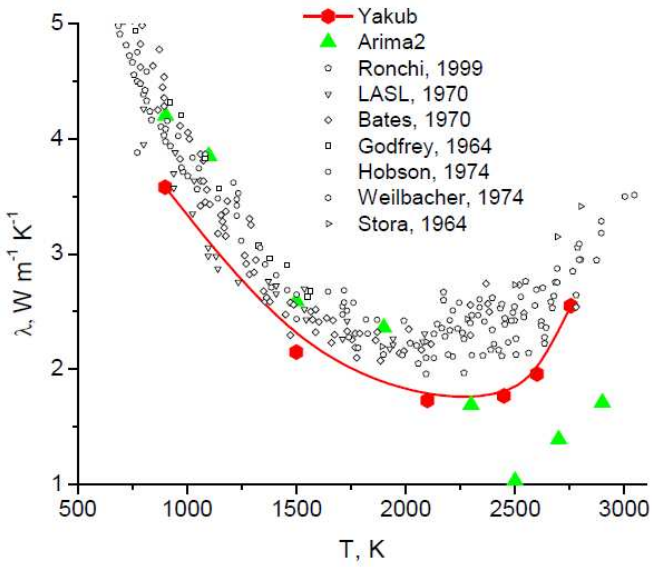

Figure 5. Thermal conductivity of stoichiometric UO_2 in the range of 500-3000K. Experimental data taken from [13].

Ionic electric conductivity was calculated using eq. (11). The data for Yakub potential is present on fig. 6.

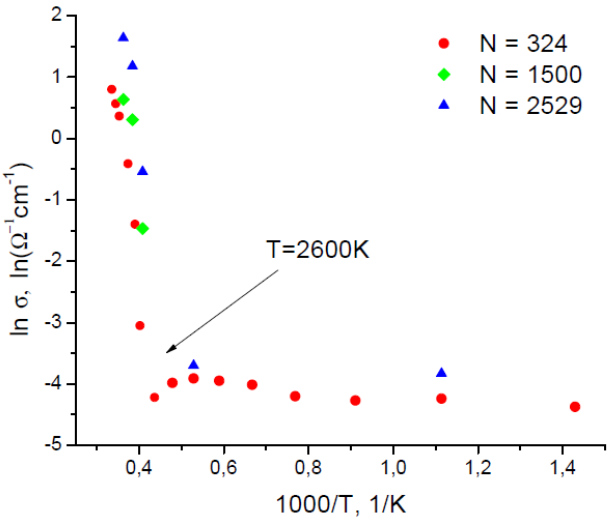

Figure 6. Ionic conductivity of stoichiometric UO_2.

3.3. High-temperature Structure

We additionally examined the possibility of melting of one of sublattices. The technique entails initial de-equilibration of the system by displacing oxygen ions far from their positions (at distances more than 0.1*a* where *a* is the lattice constant). Practically, this imitates a liquid state of the oxygen sublattice. If the state is stable, the system will exhibit a liquid state of one (or both) of sublattices. In the other case it will return to the crystalline state. In order to determine if melting is possible we calculated radial distribution functions $g_{\alpha\beta}(r) = \frac{V}{N}\frac{n_\beta(r)}{4\pi r^2 \Delta r}$ ($n_\beta(r)$ is the average quantity of ions of type β that are found at distances between r and $r+\Delta r$ from the α type ion). The results are presented on fig. 7. Calculations were made for system size 5x5x5 (1500 ions).

Also, calculations of radial distribution functions of lattice with a Frenkel defect was made. The result are show on fig. 8.

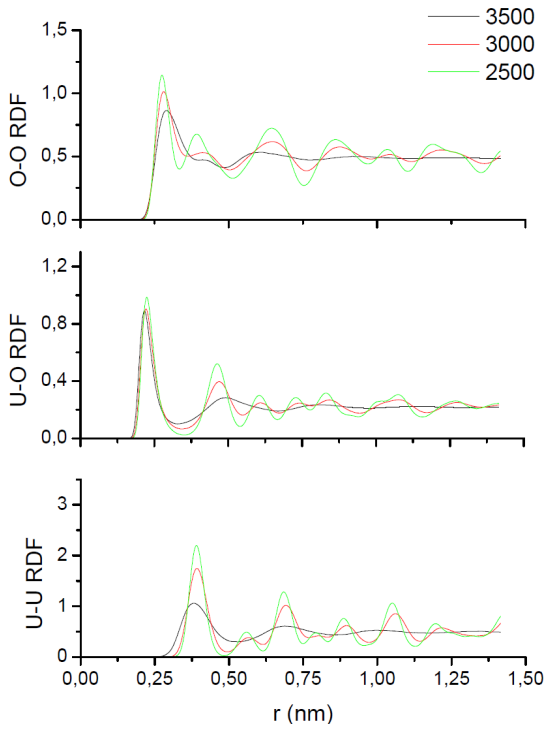

Figure 7. Temperature dependence of radial distribution functions (RDF) for each pair of species.

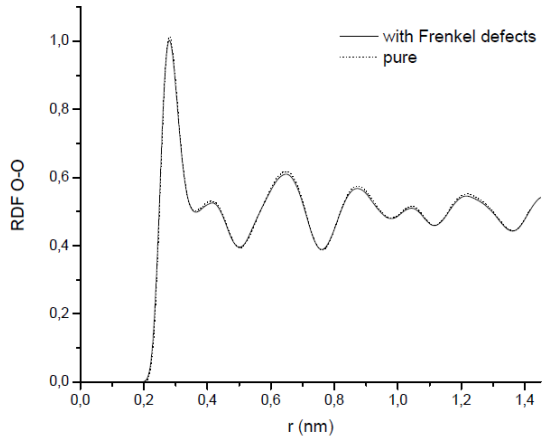

Figure 8. Influence of Frenkel-type defects on the radial distribution function O-O in a non-perturbed system at 3000 K.

To illustrate the mobility of ions, real-time shots were taken directly from MD simulation after $20x10^3$ steps. The resulting images are placed in fig. 9.

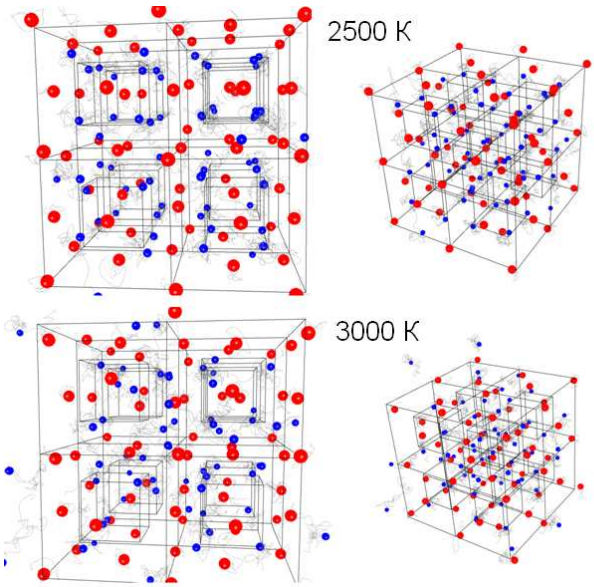

Figure 9. High-temperature lattice structure of UO_2.

Finally, typical oxygen ion trajectories at 3000 K are presented on fig. 10.

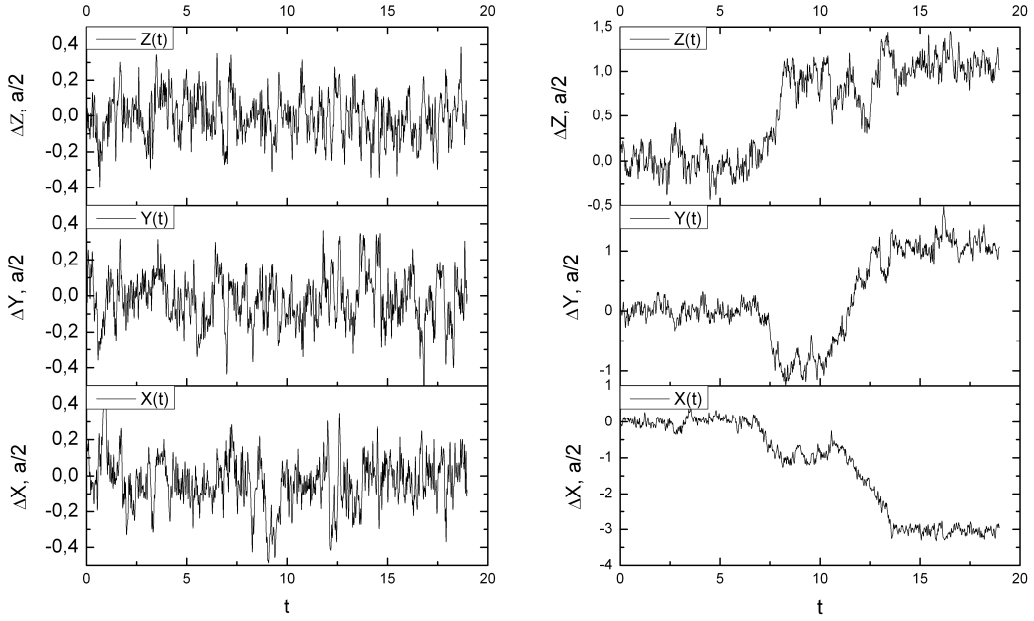

Figure 10. Typical oxygen trajectories at 3000 K.

4. CONCLUSIONS

Fig. 2 shows that Arima1 potential gives very poor results. We think that it is due to the innate defects of the potential form (2): it uses formal charges and doesn't account for ionicity, moreover. the potential has unphysical behavior when *r* is close to zero. Arima2, Basak and Yakub seem to reproduce experimental data more correctly.

Fig. 3 shows that heat capacity is better represented by Yakub potential. Both Yakub and Arima2 potentials show the presence of a peak on heat capacity which is similar to the feature of a system with second order phase transition. Closer examination shows that the peak temperature is related to the beginning of thermal and ionic conductivity rise on fig. 5 and 6, correspondingly.

Fig. 4 shows that Arima1 potential fails to describe thermal conductivity in uranium dioxide. Arima2, Yakub and Basak show very reassuring results above Debye temperature. Basak potential, however, tends to underestimate thermal conductivity at temperatures close to 2000 K.

Such ionic conductivity behavior as depicted on fig. 6 is peculiar because it is often found in superionic conductors. However, fig. 7, 9 and 10 show that there are no signs melting of one of sublattices. On the contrary, radial distribution functions show that both sublattices are stable below 3000 K. The result on fig. 8 shows that Frenkel defects do not modify the radial distribution functions. But in fact, oxygen ions are indeed very mobile. As shown on fig. 10, thermal vibrations are very high and some ions move through <111> directions inside the unit

cell. In addition, oxygen can escape its native unit cell and move to a position in the neighboring cell – shown as <110> transition. These facts resemble kick-out diffusion.

We conclude that a new mechanism for lattice thermal conductivity rise in UO_2 at very high temperatures was found.

REFERENCES

1. P. Sidzingre and M.J. Gillan, "A Molecular Dynamics Study of Solid and Liquid UO_2," *J. Phys. C: Solid State Phys*, **Vol. 21,** pp. 4017-4031 (1988).
2. R. Kubo, M. Toda, N. Hashitsume, *Statistical Physics II. Nonequilibrium Statistical Mechanics*, Springer-Verlag, Berlin, Germany (1985).
3. T. Arima, et al, "Evaluation of Melting Point of UO2 by Molecular Dynamics Simulation," *J. of Nucl. Mat*, **Vol. 389,** pp. 149-154 (2009).
4. C.B. Basak, et al, "Classical Molecular Dynamics Simulation of UO_2 to Predict Thermophysical Properties," *J. of Alloy and Comp.* **Vol. 360.** pp. 210-216 (2003).
5. K. Govers, et al, "Comparison of Interatomic Potentials for UO_2. Part I: Static Calculation," *J. of Nucl. Mat.* **Vol. 366,** pp. 161-177 (2007).
6. E. Yakub, C. Ronchi, D. Staicu, "Diffusion of Helium in Non-stoichiometric Uranium Dioxide," *J. of Nucl. Mat.* **Vol. 400**, pp. 189-195 (2010).
7. A.S. Boyarchenkov, S.I. Potashnikov, "Parallel'naya Molekulyarnaya Dinamika s Summirovanium Eval'da i Integrirovaniem na Graficheskikh Processorakh," *Vichisl. Met. v Progr.*,**Vol. 10,** pp. 158-175 (2009).
8. S. Melchionna, et al, "Hoover NPT Dynamics for Systems Varying in Shape and Size," *Mol. Phys.*, **Vol. 78**, No. 3. pp. 533-544 (1993).
9. M. J. Gillan, "The Molecular Dynamics Calculation of Transport Coefficients," *Physica Scripta*, **Vol. T39,** pp. 362-366 (1991).
10. Ed. by S. Yip. *Handbook of Materials Modeling*, Springer, Dodrecht, Netherlands (2005).
11. "Thermal expansion of solid uranium dioxide," http://www.insc.anl.gov/matprop/uo2/thrm_exp/solid/expsuo2.pdf (1996).
12. "Enthalpy and heat capacity of solid uranium dioxide," http://www.insc.anl.gov/matprop/uo2/ent_hc/solid/hcpsuo2.pdf (1996).
13. "Thermal conductivity and thermal diffusivity of solid uranium dioxide," http://www.insc.anl.gov/matprop/uo2/cond/solid/thcsuo2.pdf (1996).